Nano Energy 62 (2019) 709–717

Contents lists available at ScienceDirect

Nano Energy

journal homepage: www.elsevier.com/locate/nanoen

Full paper

Tuning Li-enrichment in high-Ni layered oxide cathodes to optimize electrochemical performance for Li-ion battery

Rui Wang[a,1], Guoyu Qian[a,1], Tongchao Liu[a], Maofan Li[a], Jiajie Liu[a], Bingkai Zhang[a], Weiming Zhu[a], Shuankui Li[a], Wenguang Zhao[a], Wenyun Yang[b], Xiaobai Ma[c], Zhendong Fu[c], Yuntao Liu[c], Jinbo Yang[b], Lei Jin[d,**], Yinguo Xiao[a,***], Feng Pan[a,*]

[a] School of Advanced Materials, Peking University, Shenzhen Graduate School, Shenzhen, 518055, PR China
[b] State Key Laboratory for Mesoscopic Physics, School of Physics, Peking University, Beijing, 100871, PR China
[c] Department of Nuclear Physics, China Institute of Atomic Energy, Beijing, 102413, PR China
[d] Ernst Ruska-Centre for Microscopy and Spectroscopy with Electrons, Forschungszentrum Jülich GmbH, 52425, Jülich, Germany

ARTICLE INFO

Keywords:
Li-enrichment
Layered oxide
Li/Ni exchange
Structural characterization
Electrochemical performance

ABSTRACT

To understand what and how structural properties affect battery performance, and to optimize the structural properties accordingly are of crucial importance to improve the performance of cathode materials for advanced Li-ion batteries. Herein, we investigated the influence of Li-enrichment in $Li_{1+x}(Ni_{0.8}Co_{0.2})_{1-x}O_2$ transition metal (TM) oxide cathodes, obtained by sintering $Ni_{0.8}Co_{0.2}(OH)_2$ precursor with different amount of Li sources. Compared with stoichiometric $Li_{1+x}(Ni_{0.8}Co_{0.2})_{1-x}O_2$ (i.e. $x = 0$, Li:TM = 1:1), the improvements of cycling stability and rate performance were observed in material with moderate degree of Li-enrichment with respect to TMs (i.e. $x = 0.019$, Li:TM = 1.04:1). Further increase in Li:TM ratio up to 1.07 diminishes the electrochemical performance. Multi-scale structural characterizations including neutron diffraction and aberration-corrected transmission electron microscopy measurements show that the Li-enrichment leads to a monotonical increase in both Li/Ni exchange ratio and Li slab space. Based on the results, we argue that, in material with moderate Li-enrichment, larger Li slab space can facilitate the diffusion of Li ions and a certain amount of Li/Ni disordering can also mitigate the contraction of layered structure, therefore resulting in an optimized electrochemical performance; while in material with excessive Li:TM ratio, the diffusion path can be partially blocked due to the presence of redundant Ni ions in Li layers.

1. Introduction

Lithium-ion batteries (LIB) are considered as ideal and promising power sources, which possess extensive applications, such as portable electronics, electric vehicles and power storage for renewable energy sources [1-3]. Although a Li-ion battery is composed of four basic components, i.e. a negatively charged anode, a positively charged cathode, the electrolyte and the separator, the electrochemical performance of LIB is mostly dependent on the properties and type of cathode being used because the capacity of LIB relies on the amounts of Li ions that can be deintercalated from the cathode material [4,5]. Owing to the higher energy density, higher reversible capacity and lower cost compared with the traditional $LiCoO_2$, high-Ni $Li(Ni_xMn_yCo_z)O_2$ (NMC, $x + y + z = 1$ and $x > 75\%$) layered structure cathode materials have attracted tremendous amount of attention in the quest to develop appealing cathode with better electrochemical performances [6-10]. However, the presence of Li/Ni exchange is found to be a common feature in high-Ni NMC cathode materials and generally it is believed that the Li/Ni exchange will lead to structural disorder and impede the Li diffusion in Li layers, resulting in lower specific capacity and poor rate performance [11-13].

As one type of structural imperfection, Li/Ni exchange usually happens between the Li layers and transition metal (TM) layers in NMC materials during synthesis and electrochemical cycling. Previous reports have demonstrated that such Li/Ni exchange shows a great restriction on the electrochemical performance of the battery electrodes:

* Corresponding author.
** Corresponding author.
*** Corresponding author.
E-mail addresses: l.jin@fz-juelich.de (L. Jin), y.xiao@pku.edu.cn (Y. Xiao), panfeng@pkusz.edu.cn (F. Pan).
[1] These authors contributed equally to this work.

https://doi.org/10.1016/j.nanoen.2019.05.089
Received 5 March 2019; Received in revised form 19 May 2019; Accepted 31 May 2019
Available online 02 June 2019

(i) The antisite Ni^{2+} may impede the kinetics of Li diffusion (8.3% excess Ni present in the Li layer results in a 20–30 meV increase in the activation barrier) [14,15]. (ii) Li/Ni exchange may also degrade the cycling stability by inducing the anisotropic stress in the bulk structure [16]. (iii) The antisite Ni^{2+} in the Li layers may gradually migrate to the particle surface and lead to Ni depletion in the bulk. Hence, structural stability and capacity fade during electrochemical cycling [17,18]. Besides the obvious drawbacks mentioned above, other studies also show: (i) Li/Ni exchange can mitigate the slab-distance contraction at high states of charge, thereby stabilizing the structure [19,20]. (ii) Although Li/Ni exchange restricts the diffusion of Li-ions, it benefits the thermal stability of high-Ni NMC materials [21]. Based on above understandings, a balance between the negative and positive influences should be carefully considered so that an optimum degree of Li/Ni exchange for high-Ni NMC materials can be achieved in order to obtain the best electrochemical performance.

In this work, a series of high-Ni layered cathode $Li_{1+x}(Ni_{0.8}Co_{0.2})_{1-x}O_2$ with different degrees of Li-enrichment were obtained by deliberately introducing extra Li source (with respect to TMs) during the synthesizing procedures. Complementary neutron scattering and X-ray scattering investigations combined with aberration-corrected transmission electron microscopy measurements were performed in order to probe the microstructural changes of all samples and to get insights into the variation of Li/Ni exchange ratio and the lattice parameters. It was found that both Li/Ni exchange ratio and lattice parameters in $Li_{1+x}(Ni_{0.8}Co_{0.2})_{1-x}O_2$ exhibit a gradual increase with increasing degree of Li-enrichment (with respect to TMs). In contrast to the stoichiometric $LiNi_{0.8}Co_{0.2}O_2$ and over-Li-doped $Li_{1+x}(Ni_{0.8}Co_{0.2})_{1-x}O_2$ (e.g., $x = 0.034$), the better cycling and rate performances were achieved for the optimal-Li-doped $Li_{1+x}(Ni_{0.8}Co_{0.2})_{1-x}O_2$ with $x = 0.019$. This can be attributed to the balance between the negative and positive influences of Li/Ni exchange ratio and Li-slab space on lithium diffusion. Our results demonstrate that tuning Li-enrichment is an effective approach to optimize the electrochemical performance in high-Ni layered oxide cathodes based on the relationship between structural properties and electrochemical performances.

2. Experimental section

2.1. Sample synthesis

The precursor $Ni_{0.8}Co_{0.2}(OH)_2$ was synthesized using a coprecipitation method. First, 0.5 mol/L $NiSO_4$ and $CoSO_4$ aqueous solution with stoichiometric ratio were gradually added into the three-necked flask with stirring constantly under the protection of N_2 atmosphere. Then, NaOH solution and $NH_3{\cdot}H_2O$ solution were simultaneously added to the three-necked flask through a micro-injection pump under the same atmosphere. After reacting for 8 h, the precipitate was washed several times by deionized water to reduce the pH to 7. Later on it was separated by centrifugalization and dried under vacuum at 393 K. The dried precursor was mixed with a certain proportion of $LiOH{\cdot}H_2O$, ground sufficiently, and calcined under an O_2 atmosphere at 753 K for 8 h. Subsequently, the calcined mixture was heated to 1023 K and stayed for 15 h to ensure sufficient reaction. Finally, the samples were air cooled to room temperature. Here, three $Li_{1+x}(Ni_{0.8}Co_{0.2})_{1-x}O_2$ cathode samples with different degrees of Li-enrichment (relative to TMs) were obtained by setting the nominal ratio between $LiOH{\cdot}H_2O$ and $Ni_{0.8}Co_{0.2}(OH)_2$ precursor to 1:1, 1.1:1, and 1.2:1, respectively. This yields samples with determined x of 0, 0.019 and 0.034, respectively, as discussed later. In the following we label them as S0, S10 and S20 for clarity. The morphology of $Ni_{0.8}Co_{0.2}(OH)_2$ precursor and as-prepared $Li_{1+x}(Ni_{0.8}Co_{0.2})_{1-x}O_2$ samples is shown in Fig. S1.

2.2. Electrochemical measurements

Electrochemical testing was performed by assembling a button cell (2032). The prepared positive electrode material was dissolved in NMP together with acetylene black and PVDF in a ratio of 8:1:1 to prepare a slurry, which was then coated on an aluminum foil. After dried in an oven at 353 K, the coated foil was cut into discs as pole piece with diameter of 1 cm. The pole piece was then transferred to a vacuum oven at 393 K for overnight drying. Remove the pole piece into glove box and install the battery. The electrolyte was 1 M $LiPF_6$ in EC: EMC: DMC (1:1:1 in volume), the membrane used Celgard 2500, and the negative electrode is lithium metal. The cells were tested on a battery cycler (Neware Test System) and an electrochemical workstation (CHI660C). The cycle performance was measured at 1C from 2.7 V to 4.5 V at room temperature (RT). The rate performance was measured at 0.1C, 0.2C, 0.5C, 1C, 2C, 5C from 2.7 V to 4.5 V at RT. The electrochemical impedance spectroscopy (EIS) was measured in open circuit voltage with frequency ranging from 0.01 Hz to 100 kHz.

2.3. Structural characterization

The X-ray diffraction (XRD) patterns of the polycrystalline samples were collected by using Bruker D8 ADVANCE diffractometer with Cu K_α radiation at room temperature. Neutron powder diffraction (NPD) experiments were performed on Peking University High Intensity Powder Diffractometer (PKU-HIPD) at China Institute of Atomic Energy (CIAE). The powder samples were loaded in cylindrical vanadium sample holders and mounted in a sample changer for room temperature measurements. A Si(115) monochromator was used to produce a monochromatic neutron beam of wavelength 1.478 Å. A combined Rietveld refinement method is adopted to analysis the NPD patterns with step size of 0.05° and XRD patterns with step size of 0.05° simultaneously by using program FULLPROF suite [22]. The Pseudo-Voigt function is used to model the peak profile shape of both NPD and XRD patterns properly and high enough counting statistics make the refinement of the crystal structures of all compounds much more reliable.

The samples were sonicated in ethanol for about 5 min and then dropped onto a lacy-carbon-coated Cu multigrid for scanning transmission electron microscopy (STEM) investigations. High-angle annular dark-field (HAADF) STEM imaging was carried out on an FEI Titan G2 ChemiSTEM 80–200 transmission electron microscope [23] equipped with an ultra bright field-emission gun and a spherical aberration correction system for the electron probe, enabling structures to be probed with a spatial resolution better than 80 p.m. The microscope was operated at 200 kV. The convergence semi-angle for STEM imaging is approximately 25 mrad, while the collection semi-angle is about 70–200 mrad. In order to minimize the possibility of electron beam induced sample damage and/or structural transformations, a fresh sample area (i.e. without beam illumination prior to the image acquisition) was always used and a very short dwell time (about 1 μs/pixel) was applied during image acquisition. The sample element ratio was tested by ICP (Inductively coupled plasma optical emission spectrometry, JY2000-2, Horiba Jobin Yvon). The valence states of the transition metal elements Ni and Co were probed by X-ray photoelectron spectroscopy (XPS) on ESCA Lab220I-XL with monochromatic Al Kα X-ray source, and all the binding energy are calibrated with C 1s signal at 284.8 eV.

3. Experimental results

3.1. Electrochemical performance

Fig. 1a shows Galvanostatic charge-discharge profiles of full batteries fabricated with S0, S10 and S20 electrodes at the first cycle. The initial specific discharge capacities, operated between 2.7 V and 4.5 V with 0.1C, are 219.9 $mAh{\cdot}g^{-1}$, 222.0 $mAh{\cdot}g^{-1}$, 210.3 $mAh{\cdot}g^{-1}$, and the first cycle Coulomb efficiency are 89.9%, 90.2%, 87.7%, respectively. To evaluate the cyclic stability of the as-prepared batteries with different degrees of Li-enrichment, the cycling performances are also

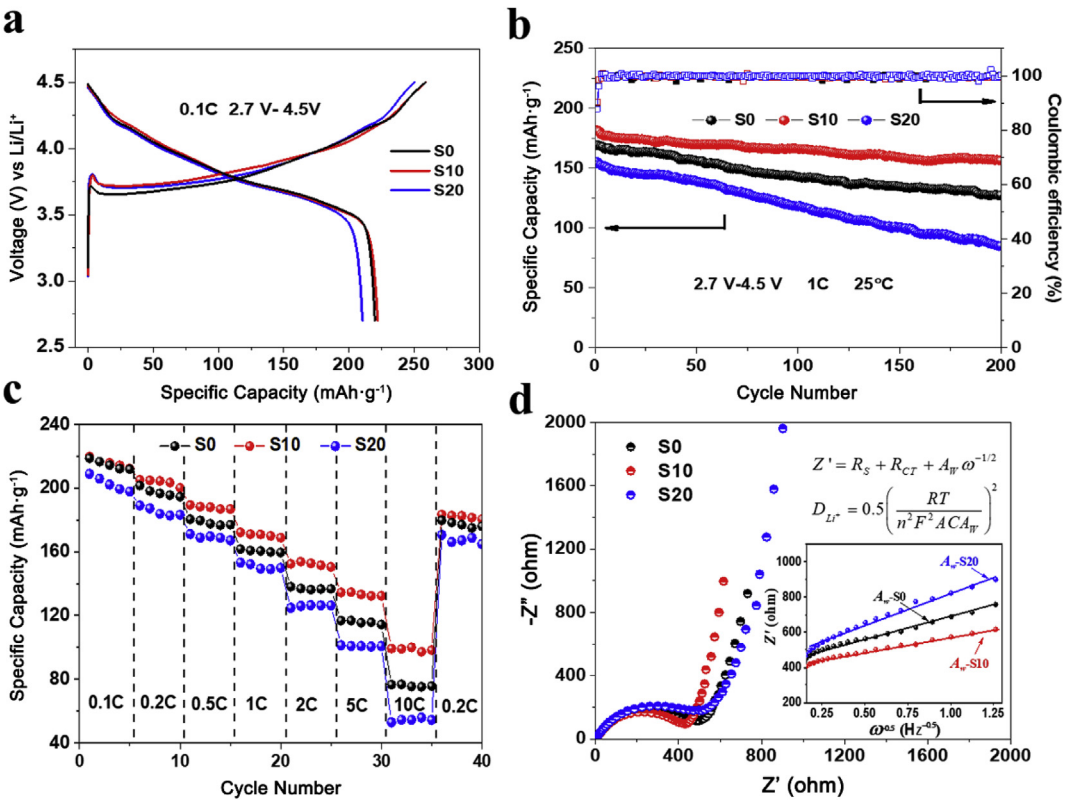

Fig. 1. Electrochemical properties of full cells fabricated by S0, S10 and S20 cathode. (a) First cycle charge-discharge curves of 0.1C rate in a voltage window of 2.7 V-4.5 V for S0, S10 and S20. (b) Cycling performance at 1C rate in a voltage window of 2.7 V-4.5 V for S0, S10 and S20. (c) Rate performance in a voltage window of 2.7 V-4.5 V of S0, S10 and S20. (d) Nyquist plots before charge and discharge of S0, S10 and S20. The inset is Z′-$\omega^{-1/2}$ diagram of S0, S10 and S20.

investigated for 200 cycles at 1C in Fig. 1b. Stoichiometric S0 cathode delivers an initial discharge capacity of 169.3 mAh·g^{-1} and has a capacity retention over 75%. In comparison, the S10 cathode retains over 85 % of its initial capacity (181.8 mAh·g^{-1}) with a stable Coulombic efficiency above 99.9%, which exhibits the best cycling property among three cathodes. In addition, the S20 cathode suffers from an obvious capacity fade (less than 55% capacity retention) after 200 cycles, indicating that a moderate degree of Li excess in high-Ni cathode materials has a significant effect in terms of enhancing the cycling performance.

Moreover, rate performance was studied for all three electrodes at different charge-discharge rates (0.1C, 0.2C, 0.5C, 1C, 2C, 5C, 10C, respectively) between the potential window of 2.7 V-4.5 V. The results are shown in Fig. 1c. Initially, there are few differences among three cathode electrodes at low current rates (0.1C and 0.2C). When charge-discharge rates increase to 10C, the discharge capacity of S0, S10, S20 cathodes are 78 mAh·g^{-1}, 92 mAh·g^{-1} and 55 mAh·g^{-1}, respectively. For S10 cathode, when the current rate increases to almost 100 times (from 0.1C to 10C), it still remains a capacity retention of 41.6%, indicating a superior Li-ion diffusion property.

To get insight into the Li-ion transport behavior of the high-Ni cathodes with excess Li content, the EIS is carried out for the initial S0, S10 and S20 electrodes and the results are presented in Fig. 1d, in which a high-frequency semicircle and a low-frequency tail are observed. The semicircle is associated with the surface charge transfer process (R_{ct}) [24]. The R_{ct} before cycling is progressively increased in the order of S10, S0 and S20 electrodes, which indicates that the full battery fabricated by S10 cathode has the minimum internal impedance with the best cycling stability. On the other hand, the low-frequency tail is associated with the Li-ion diffusion process in the active electrode particles, and the slope of the tail corresponds to a Warburg diffusion [25]. The Warburg coefficient A_w has been shown in the inset of Fig. 1d, and the calculation details are described in Supporting Information (Fig. S2). As the Li-ion diffusion coefficient is inversely proportional to the Warburg coefficient [25], the S10 cathode demonstrates the largest Li-ion diffusion ability with the smallest Warburg coefficient among three electrodes. Hence, it can be concluded that appropriate degree of Li-enrichment in $Li_{1+x}(Ni_{0.8}Co_{0.2})_{1-x}O_2$ cathodes, such as in S10, contributes to the overall enhancement of electrochemical performance including specific capacity, cycling stability, rate performance and Li-ion diffusion ability, while excessive degree of Li-enrichment as shown in S20 leads to obvious reduction of electrochemical characteristics.

3.2. Structural characterizations

Why there exists an optimum degree of Li-enrichment for high-Ni $Li_{1+x}(Ni_{0.8}Co_{0.2})_{1-x}O_2$ materials with superior electrochemical performance? As mentioned in the introduction section, Li/Ni exchange has great impact on the electrochemical performance of layered NMC materials. Thus, a quantitative investigation on the structural properties at the atomic level and a comprehensive explanation on how these microstructural features affect the performance are necessary. They will be demonstrated in the following.

Given the fact that electrochemical performance of cathode materials is largely depends on its structural characteristics, such as the spatial distribution and antisite exchange of ions, we performed detailed studies on average and local structure with complementary XRD, NPD and STEM methods. Because neutron diffraction method possesses not only high sensitivity to atoms of light element but also the ability to differentiate Ni from Co, the atomic positions and the site occupancies of all atoms in $Li_{1+x}(Ni_{0.8}Co_{0.2})_{1-x}O_2$ can be precisely determined. In contrast, X-ray diffraction method is not sensitive to light element such as lithium and oxygen, nevertheless, it can be used to deduce accurate lattice constants of samples by taking advantage of the intrinsic high

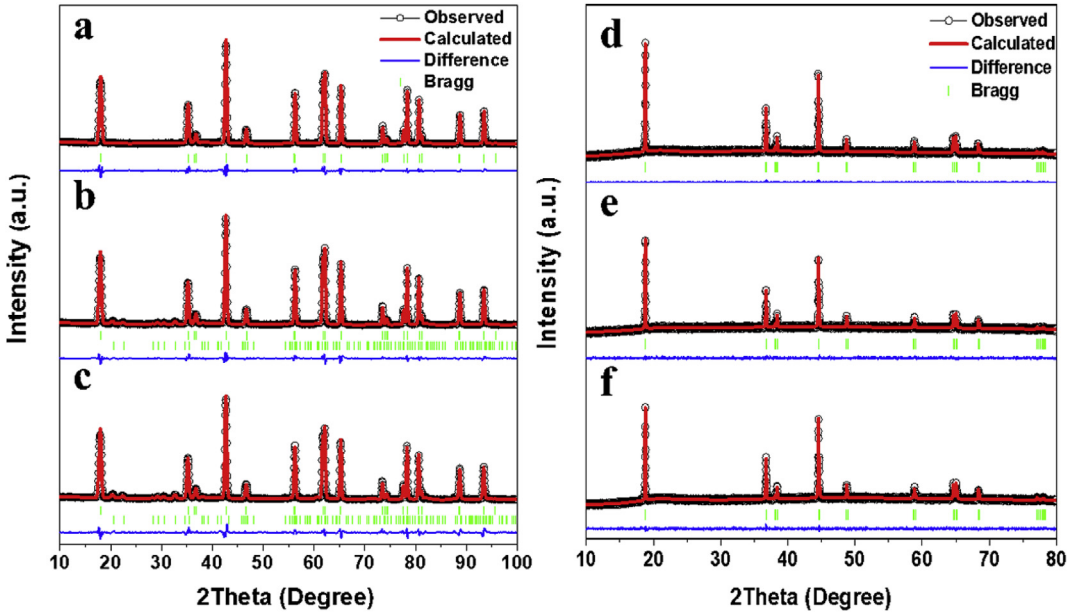

Fig. 2. Neutron powder diffraction refinement patterns for (a) S0, (b) S10 and (c) S20. XRD patterns of (d) S0, (e) S10 and (f) S20. The circles represent the observed intensities, the solid line is the calculated pattern. The difference between the observed and calculated intensities is shown at the bottom. The Bragg reflection positions of layered cathode materials are indicated by the vertical bars. In (b) and (c), the Bragg reflection position of Li_2CoO_3 impurities are also indicated by vertical bars at a lower position.

resolution of X-ray radiation. Therefore, the combined refinement including both NPD and XRD profiles are performed in order to obtained accurate structural information. The refined NPD and XRD patterns are presented in Fig. 2 and the deduced structural parameters are given in Table S1. Apparently, all $Li_{1+x}(Ni_{0.8}Co_{0.2})_{1-x}O_2$ samples, as expected, crystallize in the rhombohedral structure with space group *R-3m*. A small amount of Li_2CO_3 impurities were observed in Li-enrichment samples (S10 and S20), as the lithium carbonate cannot be well inhibited in practical production. As illustrated in Fig. S3, the lattice parameters and the volume of high-Ni $Li_{1+x}(Ni_{0.8}Co_{0.2})_{1-x}O_2$ cells exhibit gradually increments with the integration of excess Li contents (from S0 to S20), indicating that the enriched Li is incorporated into the lattice of pristine material, thus forming a single phase solid solution. Such founding is considered to be associated with the Li/Ni exchange as well.

By adopting above rhombohedral structural model and taking into account the atomic occupation of excess Li, the crystallographic formula for all three samples are deduced. As shown in Table 1, the ratio between Li and TM increases from 1 in S0 (i.e. $x = 0$) to 1.04 in S10 ($x = 0.019$), and further to 1.07 in S20 ($x = 0.034$), indicating the increased degree of Li over-stoichiometry. Accompanied with the increase of Li content, the Li/Ni exchange ratio rises accordingly. For instance, the ratio of Ni located at Li layers (i.e. at 3b Wyckoff site) increase from 1.2% in S0 to 3.0% in S10, and further to 5.2% in S20.

In general, the Li^+/Ni^{2+} exchange takes place as an inevitable structural characteristic due to the similar radii between Li^+ and Ni^{2+} ions ($r_{Ni}2+ = 0.69$ Å, $r_{Li}+ = 0.76$ Å), as well as the existence of magnetic frustration and super-exchange interaction [26,27]. Moreover, the low energy barrier of Ni^{2+} migration from the 3a Wyckoff site in TM layers to 3b site in Li layers further facilitates the Li/Ni exchange kinetically [28,29]. However, for high-Ni $LiNi_{0.8}Co_{0.2}O_2$ materials, where most Ni cations are much smaller Ni^{3+} ($r_{Ni}3+ = 0.56$ Å), the steric effect of cationic size cannot explain why Li/Ni exchange happens even more frequently in high-Ni NMC materials [18]. Pan et al. proposed that the super-exchange interactions exist among TMs and might provide a new driving force in tuning the Li/Ni exchange [27]. As for high-Ni $Li(Ni_{0.8}Co_{0.2})O_2$, most of antisite Ni ions are in the 3 + valence state in the TM layers. Once the Ni ion in TM layers exchanges with Li ion in Li layers, the valence state of antisite Ni ion will change to 2+. Consequently, the nearest Co in TM layers will change its valence state from Co^{3+} to Co^{4+} to make charge compensation at the same time [30,31].

In order to prove the above scenario, the valence and proportion of the TM elements are investigated by XPS. Fig. 3a-c shows the Ni $2p_{3/2}$ energy levels of (a) S0, (b) S10, (c) S20, and the Gauss-Lorentz curve is used to fit the profiles of nickel ions and to get their corresponding forbidden band energies. Proportions of various TM ions deduced from XPS data are listed in Table S3. It clearly shows that the proportion of Ni^{2+} increase gradually with the increase in the degree of Li-enrichment, whereas the proportion of Ni^{3+} decreases correspondingly. Fig. 3 d-f shows the XPS profile of Co 2p energy levels, in which the binding energy of $2p_{3/2}$ is fitted by the Gauss-Lorentz curve of the profiles of Co^{4+} and Co^{3+}, and it can be also clearly observed that Co^{4+} exist and the content of Co^{4+} is raising with increasing degree of Li-enrichment (from S0 to S20) According to the XPS results, the ratios of Ni^{2+}/Ni^{3+} and Co^{4+}/Co^{3+} are raising with increasing degree of Li-enrichment (from S0 to S20), which is in consistent with our previous assumption and conclusions [27], *i.e.* the amount of Ni^{2+} and Co^{4+} increases with

Table 1
Crystallographic Formulas with atomic occupation at each site, molar ratios of Li:Ni:Co and Li/Ni exchange ratios in high-Ni $Li_{1+x}(Ni_{0.8}Co_{0.2})_{1-x}O_2$ series deduced from XRD and NPD combined refinement for S0, S10 and S20. The subscript 3a and 3b denotes Wyckoff positions.

Sample	Crystallographic Formula with atomic occupation at each site	Molar ratios of Li:Ni:Co	Li in Ni layer%	Ni in Li layer%
S0	$(Li_{0.988}Ni_{0.012})_{3b}$ $(Li_{0.012}Ni_{0.788}Co_{0.20})_{3a}O_2$	1:0.8:0.2	1.2(4)	1.2(4)
S10	$(Li_{0.970}Ni_{0.030})_{3b}(Li_{0.049}Ni_{0.755}Co_{0.196})_{3a}O_2$	1.039:0.8:0.2	4.9(4)	3.0(4)
S20	$(Li_{0.948}Ni_{0.052})_{3b}(Li_{0.086}Ni_{0.720}Co_{0.193})_{3a}O_2$	1.070:0.8:0.2	8.6(4)	5.2(4)

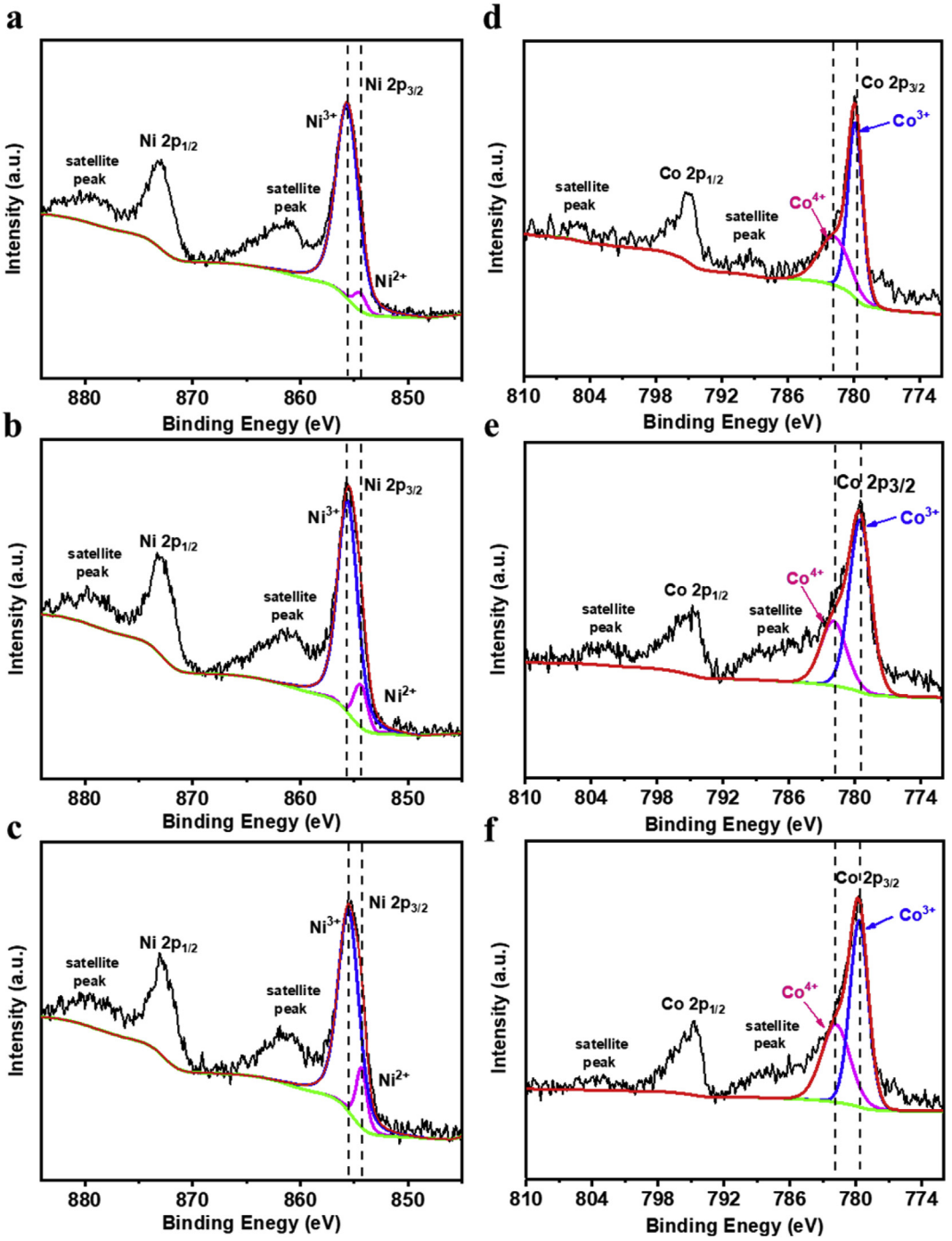

Fig. 3. XPS patterns of Ni $2p_{3/2}$ of Ni^{2+}, Ni^{3+} for (a) S0, (b) S10, (c) S20 and Co $2p_{3/2}$ for (d) S0, (e) S10, (f) S20. Satellite peaks for Ni 2p levels are also marked.

increasing Li/Ni exchange ratio in NMC materials.

As shown in Table 1, the Li/Ni exchange ratio is 1.2(4)% for S0 sample, i.e. about 1.2% Li^+ resides on Ni^{2+} site and vice versa. As a consequence of Li excess during sample preparation, the proportion of Ni at Li site increases to 3.0(4)% and 5.2(4)% for S10 and S20, respectively. The substantial variation in the contents of Li/Ni exchange ratio will certainly change not only average structure but also the local structure surrounding the Li^+, thus affecting the electrochemical performance of layered cathode materials accordingly.

Atomic-resolution HAADF STEM is used to explore the distribution of different atoms in the local area, especially to visualize the stack of Li and TMO_6 slabs along the ***c***-axis in layered $Li_{1+x}(Ni_{0.8}Co_{0.2})_{1-x}O_2$ samples. Note that the irradiation of high-energy electrons might induce atomic displacements and result in the formation of Li or O vacancies in layered cathode $Li_{1+x}Ni_{0.8}Co_{0.2}O_2$ materials, special cautions have been taken during STEM measurement in order to avoid the spurious imaging and to obtain real structure of samples, as mentioned in Section 2.3. Fig. 4 shows representative HAADF STEM images viewed along the ***b*** zone axe (i.e. [$\bar{1}2\ \bar{1}0$] axis). The alternate stack of Li and TMO_6 slabs, which are schematically highlighted in Fig. 4g-i, are clearly observed. Since the brightness of HAADF STEM images directly reflects the atomic number of an atomic column, it can be expected that only the TM (i.e. Ni/Co) columns (occupying 3b sites) are visible in a bulk $LiNi_{0.8}Co_{0.2}O_2$. In Fig. 4a-c, the continuous dots contrast in the TM layers demonstrates that the Ni/Co elements are homogeneously distributed throughout the TM layers in all three samples. As for the Li

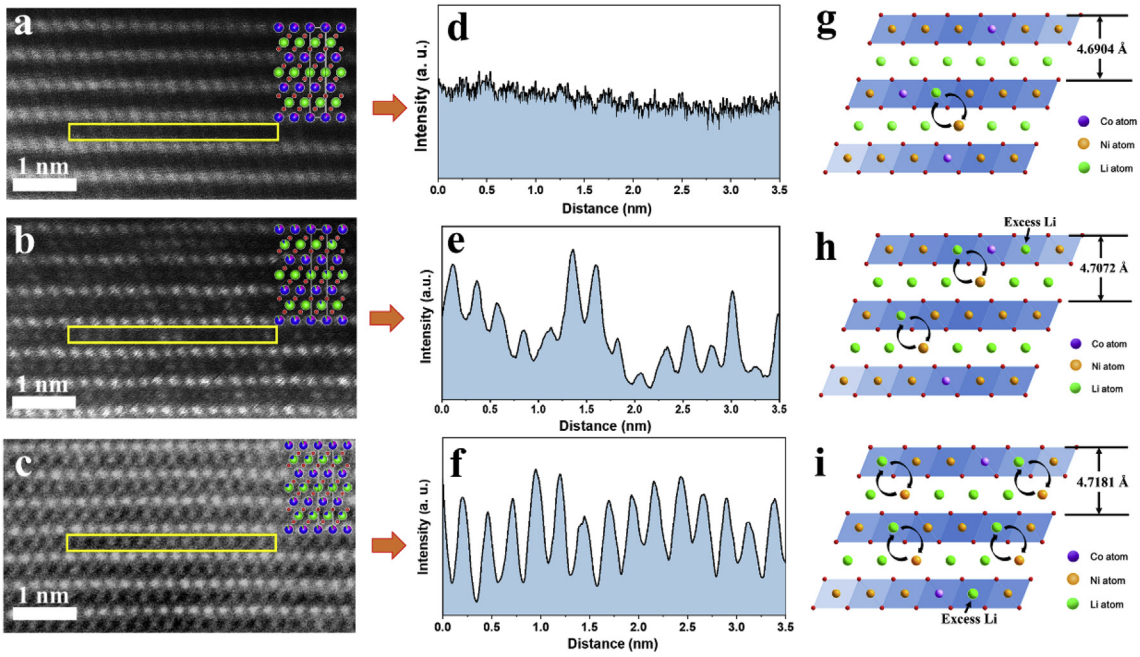

Fig. 4. Atom-resolved HAADF STEM images of (a) S0, (b) S10, (c) S20. The intensity plots of (d) S0, (e) S10, (f) S20 along the rectangular area shown in (a), (b) and (c), respectively. The schematic diagram of (f) S0, (g) S10, (h) S20, indicating the concentration of Li/Ni exchange ratio and expansion of Li-slab space.

layers, the Li atoms are nearly invisible in S0 sample as demonstrated by the HAADF line profile in Fig. 4d. Interestingly, the discontinuous dots contrast are detected in the Li layer of S10 sample, signaling the inhomogeneous occupancy of Ni at Li site with considerable concentration. This phenomenon confirms the structure characters of $Li_{1+x}(Ni_{0.8}Co_{0.2})_{1-x}O_2$ deduced from XRD/NPD results, i.e. the antisite exchange between Ni and Li becomes significant with increasing content of excess Li. Compared to S10, the number of Ni atoms at Li site further increases and exhibits nearly uniform distribution in atomic level, as shown in Fig. 4f. Moreover, the HAADF-STEM images also demonstrated that the atomic distances along both ***a*** and ***c*** axes are expanded with increasing Li/Ni antisite ratio (Fig. S4 and S5), and agree well with the XRD/NPD observations.

4. Discussion

It is reasonable and fairly to understand the origin of the various electrochemical performance in samples from aspects of their structural characteristics. Volcano-shaped evolution of the rate performance and cycling stability with increasing excess Li content in $Li_{1+x}(Ni_{0.8}Co_{0.2})_{1-x}O_2$ cathodes (Fig. 1) are intimately related to the variation of structural characters, such as Li-slab space and Li/Ni exchange ratio. First, the lattice constants of $Li_{1+x}(Ni_{0.8}Co_{0.2})_{1-x}O_2$ increases in an isotropic manner upon the integration of excess lithium. Compared with pristine S0 sample the lattice constant *a* and *b* expand from 2.8606 to 2.8618 Å with a change of 0.04%, whereas *c* expands from 14.1345 to 14.1434 Å with a change of 0.06%, resulting in an expansion in lattice volume. The isotropic change of *a*/*b* and *c* directly reflect the elongation of both intralayer and interlayer bonds attribute to the integration of Li^+ with relatively larger ionic radius. Besides, the coulomb interaction between two oppositely charged segments, i.e. positively charged Li layers and negatively charged TM layers, certainly involves in the expansion of lattice along crystallographic ***a*** and ***c***-axis when more Ni^{2+} are replaced by Li^+. Moreover, the strengthening of intralayer superexchange interactions between TM ions might also play a role in the intralayer expansion.

It is clear that larger space between these oxygen layers substantially reduces the activation energy for Li diffusion [14], and Ceder et al. have proposed that the Li slab space expansion would contribute to the faster migration/motion of Li ions as well as the enhanced rate performance of as-prepared cathodes [15]. However, with the increasing degree of Li/Ni exchange, the antisite Ni^{2+} in the Li layer is detrimental to the rate performance by blocking the lithium diffusion path and impeding the Li-ion extraction from the Li layers [27]. In addition, for the same composite of layer oxide materials such as $Li(Ni_{0.5}Mn_{0.5})O_2$, the calculation results show that 8.3% Li/Ni exchange would reduce the Li slab space reduces from 2.64 Å to 2.62 Å, which results in a 20–30 meV increase in the activation barrier [14] and a low rate capability [32]. These critical factors mentioned above are thought to be responsible for the fluctuant rate performance from S0 to S20 cathodes.

For the cycling performance, excessive expansion of Li slab space for the high-Ni $Li_{1+x}(Ni_{0.8}Co_{0.2})_{1-x}O_2$ cathodes at highly delithiation would lead to a very unstable situation and structural collapse [19,20], some degree of disorder can mitigate the slab-distance contraction at high states of charge, thus benefiting the structural stability during electrochemical cycling [20,33]. On the contrary, both the Coulombic interaction and super-exchange interaction will give rise to the distortion force and lead to the anisotropic stress in the bulk structure, which may result in irreversible crystal structure transformation during cycling [16]. Last but not least, the antisite Ni^{2+} ions in the Li layer would gradually migrate to the particle surface due to the low energy barrier for Ni^{2+} migration, leading to Ni depletion in the bulk, structural instability, and consequently cathode voltage and capacity fade [17,18], which is corresponding to the cycling property of S20 cathode. In addition, with a large degree of Li/Ni disorder, the lithium ions surrounded by nickel ions in the Li layers would be isolated from the active domain which is available for lithium diffusion (Fig. S8), the lower specific capacity of the S20 electrode compared to S0 and S10 cathodes during the initial cycle could be partially attributed to the existence of dead Li in the isolated domain.

Generally, Li/Ni exchange adversely affects diffusion of Li-ions in Li layer, but certain amount of Li/Ni exchange leads to the lattice expansion and enhances the rate performance in turn. Although lots of works attempted to suppress the Li/Ni exchange because the anisotropic stress and Ni depletion would lead to capacity fade, some degree of disordering can mitigate the slab-distance contraction at highly electrochemical delithiation, which is benefit to the cycling stability of

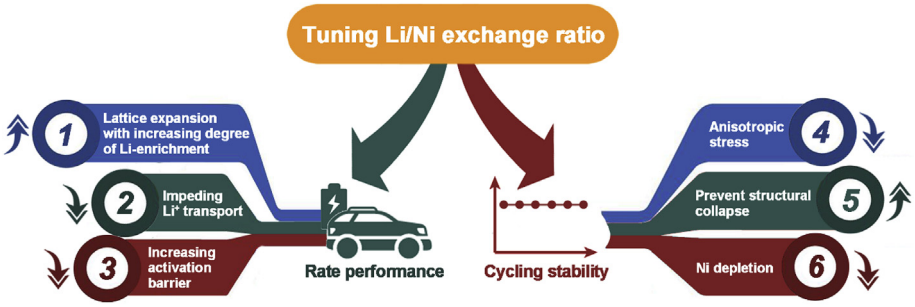

Scheme 1. The positive influences (upward arrow) and negative influences (downward arrow) of Li/Ni exchange on the electrochemical performance.

Li-enrichment high-Ni $Li_{1+x}(Ni_{0.8}Co_{0.2})_{1-x}O_2$ cathodes. Scheme 1 has been employed to demonstrate the coupling relations between the electrochemical properties and detailed mechanism for the Li/Ni exchange.

5. Conclusion

In summary, three $Li_{1+x}(Ni_{0.8}Co_{0.2})_{1-x}O_2$ cathode materials with different degrees of Li-enrichment (labeled as S0, S10, S20, respectively) were fabricated by using various excessive contents of Li reactant during the synthesizing process. S10 electrode with 3.0% Ni located at Li layer exhibits a superior electrochemical performance compared with S0 (1.2% Ni-antisite) and S20 (5.2% Ni-antisite) electrodes. The superior electrochemical performance in S10 can be attributed to its optimized structural characters, such as Li-layer space and Li/Ni exchange ratio, as revealed at the atomic level by employing neutron scattering and high-resolution STEM techniques. The steric effect of the cations, kinetic conditions, lattice expansion and the structural distortion have co-influences on the electrochemical performance of the high-Ni cathode materials. Decoupling these factors would give us a better understanding to recognize the complex impact and optimize the performance of Li-enrichment high-Ni cathode materials.

Acknowledgments

R. Wang and G.Y. Qian contributed equally to this work. This work was supported by National Materials Genome Project (2016YFB0700600), Guangdong Key-lab Project (No. 2017B0303010130), and Shenzhen Science and Technology Research Grant (No. ZDSYS201707281026184).

Appendix A. Supplementary data

Supplementary data to this article can be found online at https://doi.org/10.1016/j.nanoen.2019.05.089.

References

[1] J.M. Tarascon, M. Armand, Nature 414 (2001) 359–367.
[2] V. Etacheri, R. Marom, R. Elazari, G. Salitra, D. Aurbach, Energy Environ. Sci. 4 (2011) 3243–3262.
[3] J.B. Goodenough, Y. Kim, Chem. Mater. 22 (2010) 587–603.
[4] R. Mukherjee, R. Krishnan, T.-M. Lu, N. Koratkar, Nano Energy 1 (2012) 518–533.
[5] C. Daniel, D. Mohanty, J. Li, D.L. Wood, AIP Conf. Proc. 1597 (2014) 26–43.
[6] M.S. Whittingham, Chem. Rev. 104 (2004) 4271–4302.
[7] A. Manthiram, J.C. Knight, S.-T. Myung, S.-M. Oh, Y.-K. Sun, Adv. Energy Mater. 6 (2016) 1501010.
[8] Y.-K. Sun, Z. Chen, H.-J. Noh, D.-J. Lee, H.-G. Jung, Y. Ren, S. Wang, C.S. Yoon, S.-T. Myung, K. Amine, Nat. Mater. 11 (2012) 942–947.
[9] U.H. Kim, D.W. Jun, K.J. Park, Q. Zhang, P. Kaghazchi, D. Aurbach, D.T. Major, G. Goobes, M. Dixit, N. Leifer, C.M. Wang, P. Yan, D. Ahn, K.H. Kim, C.S. Yoon, Y.K. Sun, Energy Environ. Sci. 11 (2018) 1271–1279.
[10] J. Xu, S. Dou, H. Liu, L. Dai, Nano Energy 2 (2013) 439–442.
[11] M.S. Islam, C.A.J. Fisher, Chem. Soc. Rev. 43 (2014) 185–204.
[12] J. Zheng, W.H. Kan, A. Manthiram, ACS Appl. Mater. Interfaces 7 (2015) 6926–6934.
[13] W. Liu, P. Oh, X. Liu, M.-J. Lee, W. Cho, S. Chae, Y. Kim, J. Cho, Angew. Chem. Int. Ed. 54 (2015) 4440–4457.
[14] K. Kang, Y.S. Meng, J. Bréger, C.P. Grey, G. Ceder, Science 311 (2006) 977–980.
[15] K. Kang, G. Ceder, Phys. Rev. B 74 (2006) 094105.
[16] H. Yu, Y. Qian, M. Otani, D. Tang, S. Guo, Y. Zhu, H. Zhou, Energy Environ. Sci. 7 (2014) 1068–1078.
[17] P. Yan, A. Nie, J. Zheng, Y. Zhou, D. Lu, X. Zhang, R. Xu, I. Belharouak, X. Zu, J. Xiao, K. Amine, J. Liu, F. Gao, R. Shahbazian-Yassar, J.-G. Zhang, C.-M. Wang, Nano Lett. 15 (2015) 514–522.
[18] P. Yan, J. Zheng, D. Lv, Y. Wei, J. Zheng, Z. Wang, S. Kuppan, J. Yu, L. Luo, D. Edwards, M. Olszta, K. Amine, J. Liu, J. Xiao, F. Pan, G. Chen, J. Zhang, C. Wang, Chem. Mater. 27 (2015) 5393–5401.
[19] F. Schipper, E.M. Erickson, C. Erk, J.-Y. Shin, F.F. Chesneau, D. Aurbach, J. Electrochem. Soc. 164 (2017) A6220–A6228.
[20] Y.S. Meng, G. Ceder, C.P. Grey, W.S. Yoon, M. Jiang, J. Bréger, Y. Shao-Horn, Chem. Mater. 17 (2005) 2386–2394.
[21] J. Zheng, T. Liu, Z. Hu, Y. Wei, X. Song, Y. Ren, W. Wang, M. Rao, Y. Lin, Z. Chen, J. Lu, C. Wang, K. Amine, F. Pan, J. Am. Chem. Soc. 138 (2016) 13326–13334.
[22] J. Rodríguez-Carvajal, Physica B 192 (1993) 55–69.
[23] R.S. András Kovács, J. Karsten Tillmann, Large-scale Res. Fac. 2 (2016) A43–A46.
[24] X.Y. Qiu, Q.C. Zhuang, Q.Q. Zhang, R. Cao, Y.H. Qiang, P.Z. Ying, S.G. Sun, J. Electroanal. Chem. 688 (2013) 393–402.
[25] F. Wu, J. Tian, Y. Su, J. Wang, C. Zhang, L. Bao, T. He, J. Li, S. Chen, ACS Appl. Mater. Interfaces 7 (2015) 7702–7708.
[26] Y. Xiao, T. Liu, J. Liu, L. He, J. Chen, J. Zhang, P. Luo, H. Lu, R. Wang, W. Zhu, Nano Energy 49 (2018) 77–85.
[27] J. Zheng, G. Teng, C. Xin, Z. Zhuo, J. Liu, Q. Li, Z. Hu, M. Xu, S. Yan, W. Yang, F. Pan, J. Phys. Chem. Lett. 8 (2017) 5537–5542.
[28] Y. Wei, J. Zheng, S. Cui, X. Song, Y. Su, W. Deng, Z. Wu, X. Wang, W. Wang, M. Rao, Y. Lin, C. Wang, K. Amine, F. Pan, J. Am. Chem. Soc. 137 (2015) 8364–8367.
[29] M.-J. Zhang, G. Teng, Y.-c.K. Chen-Wiegart, Y. Duan, J.Y.P. Ko, J. Zheng, J. Thieme, E. Dooryhee, Z. Chen, J. Bai, K. Amine, F. Pan, F. Wang, J. Am. Chem. Soc. 140 (2018) 12484–12492.
[30] N.A. Chernova, M. Ma, J. Xiao, M.S. Whittingham, J. Breger, C.P. Grey, Chem. Mater. 19 (2007) 4682–4693.
[31] H. Chen, J.A. Dawson, J.H. Harding, J. Mater. Chem. 2 (2014) 7988–7996.
[32] J. Bréger, N. Dupré, P.J. Chupas, P.L. Lee, T. Proffen, J.B. Parise, C.P. Grey, J. Am. Chem. Soc. 127 (2005) 7529–7537.
[33] A. Urban, J. Lee, G. Ceder, Adv. Energy Mater. 4 (2014) 1400478.

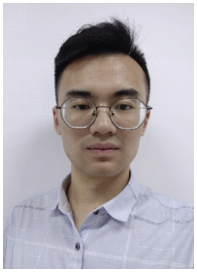

Rui Wang received his B.S. degree in Applied Physics from China University Of Petroleum (East China) in 2017. He is pursuing his M.S. degree in the School of Advanced Materials, Peking University, China. His research interest is structural characterization for cathode materials of lithium ion battery using X-ray and neutron scattering technology.

Dr. Guoyu Qian received his Ph.D. from Huazhong University of Science and Technology in 2018 and was at Columbia University as a joint Ph.D. student in 2016–2017. He is currently a postdoctoral scholar at Peking University Shenzhen Graduate School. His research interests focus on studies of lithium-ion batteries, flexible energy storage and multiferric materials.

Tongchao Liu is currently a Ph.D. candidate in Prof. Feng Pan's Group at Peking University, China. His research interests include: energy materials (battery materials, catalytic materials), nanomaterials, electrochemistry, synchrotron X-ray diffraction and X-ray absorption spectroscopy.

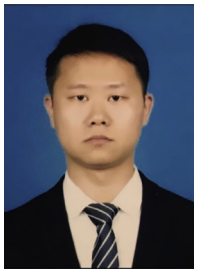

Maofan Li received his master degree in mechanics (Advanced materials and mechanics)from Peking University in 2018. His research interests mainly focus on the key materials and technologies for new energy batteries, including lithium-ion battery, sodium-ion battery and solid-state battery.

Jiajie Liu is currently a Ph.D. candidate in Prof. Feng Pan's group at Peking University Shenzhen Graduate School, China. He received his B.S. degree in Chemistry from Peking University in 2016. Currently his research interests focus on high energy density cathode materials for Li-/Na-ion batteries, especially on layered oxide materials including Li- and Mn-rich layered oxides and Ni-rich layered oxides.

Dr. Bingkai Zhang received the Ph.D. degree from Huazhong University of Science and Technology, China, in 2014. Then, He is currently a postdoctoral researcher in Peking University, China. His main research fields are computational materials design and materials for energy storage and conversion.

Weiming Zhu received his B.S. degree in Materials Science and Engineering from University of Science and Technology Beijing, P.R. China in 2017. He is pursuing his M.S. degree in the School of Advanced Materials, Peking University, P.R. China. Currently, his research interests focus on thermoelectric materials.

Dr. Shuankui Li received his Ph.D. degree in Condensed Matter Physics in 2014 from Lanzhou University, China. He is currently an Assistant Research Fellow at School of Advanced Materials, Peking University, Shenzhen Graduate School with a research focus on design and preparation high performance nanostructured thermoelectrics materials.

Wenguang Zhao is an engeneer in the School of Advanced Materials, Peking University Shenzhen Graduate School, China. He has over 10 years' experience in material characterization using wide range of analytical tools including XRD, XPS, SEM and TEM. His research interests mainly focus on the Ex/in-situ TEM and Ex/in-situ XRD characterization of battery materials.

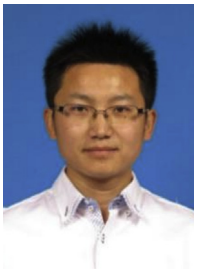

Dr. Wenyun Yang received his Ph.D. from School of Physics at Peking University, China in 2017. He was responsible for the design and construction of high intensity neutron diffractometer (PKU-HIPD) at the China Advanced Research Reactor (CARR) and is currently an instrument scientist of the PKU-HIPD. His research interests focus on application of neutron diffraction and scattering technology on new magnetic materials and other energy related materials.

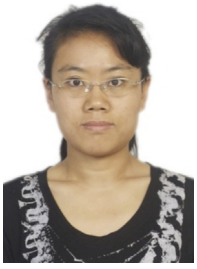

Dr. Xiaobai Ma received her Ph.D. Degree from Peking University in 2010. She was a postdoctoral fellow from 2010 to 2012 at State Key Laboratory for Mesoscopic Physics, Department of Physics in Peking University, China. In 2012, she joined China Institute of Atomic Energy as an associate professor. She is mainly engaged in neutron powder diffraction as an instrument scientist, and her research interests are magnetic materials.

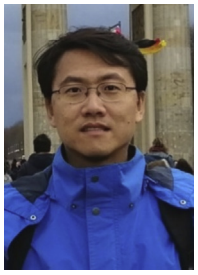

Dr. Zhendong Fu received his Ph.D. degree from RWTH Aachen University in 2011. He was a postdoc of Juelich Centre for Neutron Science from 2011 to 2017. Since June 2017 he has been a research scientist of Neutron Scattering Laboratory of China Institute of Atomic Energy. His research interests are currently focusing on magnetic materials characterization using neutron scattering techniques.

Prof. Yuntao Liu received his Ph.D. degree from Technical University Berlin in 2004. He was the director of Neutron Scattering Laboratory of Department of Nuclear Physics in China Institute of Atomic Energy (CIAE) from 2005 to 2016. Since October 2016 he became the director of Department of Radiation Metrology in CIAE. He is a professor of Graduate School of China National Nuclear Corporation and an adjunct professor of Xi'An Jiaotong University. His research interests are focusing on material characterization using neutron scattering technique.

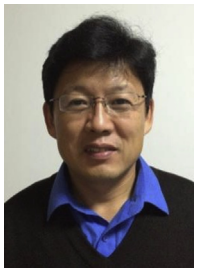

Prof. Jinbo Yang received his Ph.D. in Condensed Matter Physics from the Peking University (PKU) in 1998. He received the Alexander von Humboldt Fellowship and performed a post-doctor at IFW-Dresden Germany from 1998 to 2000. He then worked in University of Missouri-Rolla (UMR) from 2001 to 2008. He became a Professor in PKU in 2008. Prof. Yang is currently vice Dean of Institute for Condensed Matter Physics and Materials Science, School of Physics, PKU. He is leader of the Center for Magnetism and Magnetics in School of Physics. His research works focus on topics in structure and magnetism in condensed matter, including hard/soft magnets, crystal, magnetic and electronic structures of magnetic materials, nanomagnetism and spintronics. He has published more than 250 peer-reviewed SCI papers.

Dr. Lei Jin received his Ph.D. degree from School of Physics and Technology and Center for Electron Microscopy, Wuhan University, China in 2008. From 2005 to 2006, he acted as a technical assistant (exchange student) in Department of Electrical and Electronic Engineering, The University of Hong Kong, Hong Kong, China. After working shortly in Wuhan University in 2009, he was a postdoctoral researcher in the Ernst Ruska-Centre for Microscopy and Spectroscopy with Electrons, Forschungszentrum Jülich GmbH, Germany from 2009 to 2016. Since 2017, he was promoted as a tenured scientist. His research interests include quantitative high-resolution transmission electron microscopy and spectroscopy, structural defects in functional oxides and related behavior under working conditions.

Prof. Yinguo Xiao received his Ph.D. degree from Institute of Physics, Chinese Academy of Sciences, China in 2006. He was a postdoctoral fellow from 2007 to 2009 and a research scientist from 2009 to 2014 at Juelich Research Centre (Forschungszentrum Jülich), Germany. He became a tenured staff scientist in Juelich Research Centre since 2015. In 2017, he joined Peking University Shenzhen Graduate School, China as an associate professor. His research interests are on research and development of new materials for energy conversion and storage, and characterization of complex materials using X-ray and neutron scattering techniques.

Prof. Feng Pan, Chair-Professor, Founding Dean of School of Advanced Materials, Peking University Shenzhen Graduate School, Director of National Center of Electric Vehicle Power Battery and Materials for International Research, got B.S. from Dept. Chemistry, Peking University in1985 and PhD from Dept. of P&A Chemistry , University of Strathclyde, Glasgow, UK , with “Patrick D. Ritchie Prize” for the best Ph.D. in 1994. Prof. Pan has been engaged in fundamental research and product development of novel energy conversion and storage materials & devices. As Chief Scientist, Prof. Pan led 12 entities to win National Key project of Material Genomic Engineering for Solid State Li-ion Battery in China in 2016. He has been selected as one of the 2018 winner of ECS Battery Division Technology Award.